



# Increasing cloudiness in Arctic damps the increase in phytoplankton primary production due to sea ice receding

S. Bélanger<sup>1</sup>, M. Babin<sup>2</sup>, and J.-É. Tremblay<sup>2</sup>

<sup>1</sup>Université du Québec à Rimouski, Département de Biologie, Chimie et Géographie and BORÉAS, 300 allée des Ursulines, Rimouski, Québec, G5L 3A1, Canada

<sup>2</sup>Takuvik Joint International Laboratory (CNRS & ULaval), Département de Biologie, Québec-Océan and Arctictnet, Université Laval, Pavillon Alexandre-Vachon, 1045, av. de la Médecine, Québec (Québec), G1V 0A6, Canada

Correspondence to: S. Bélanger (simon.belanger@uqar.ca)

Received: 6 September 2012 – Published in Biogeosciences Discuss.: 12 October 2012

Revised: 17 April 2013 – Accepted: 14 May 2013 – Published: 20 June 2013

**Abstract.** The Arctic Ocean and its marginal seas are among the marine regions most affected by climate change. Here we present the results of a diagnostic model used to assess the primary production (PP) trends over the 1998–2010 period at pan-Arctic, regional and local (i.e. 9.28 km resolution) scales. Photosynthetically active radiation (PAR) above and below the sea surface was estimated using pre-computed look-up tables of spectral irradiance, taking as input satellite-derived cloud optical thickness and cloud fraction parameters from the International Satellite Cloud Climatology Project (ISCCP) and sea ice concentration from passive microwaves data. A spectrally resolved PP model, designed for optically complex waters, was then used to assess the PP trends at high spatial resolution. Results show that PP is rising at a rate of  $+2.8 \text{ TgC yr}^{-1}$  (or  $+14 \% \text{ decade}^{-1}$ ) in the circum-Arctic and  $+5.1 \text{ TgC yr}^{-1}$  when sub-Arctic seas are considered. In contrast, incident PAR above the sea surface (PAR(0+)) has significantly decreased over the whole Arctic and sub-Arctic Seas, except over the perennially sea-ice covered waters of the Central Arctic Ocean. This fading of PAR(0+) ( $-8 \% \text{ decade}^{-1}$ ) was caused by increasing cloudiness during summer. Meanwhile, PAR penetrating the ocean (PAR(0-)) increased only along the sea ice margin over the large Arctic continental shelf where sea ice concentration declined sharply since 1998. Overall, PAR(0-) slightly increased in the circum-Arctic ( $+3.4 \% \text{ decade}^{-1}$ ), while it decreased when considering both Arctic and sub-Arctic Seas ( $-3 \% \text{ decade}^{-1}$ ). We showed that rising phytoplankton biomass (i.e. chlorophyll *a*) normalized by the diffuse

attenuation of photosynthetically usable radiation (PUR), accounted for a larger proportion of the rise in PP than did the increase in light availability due to sea-ice loss in several sectors, and particularly in perennially and seasonally open waters. Against a general backdrop of rising productivity over Arctic shelves, significant negative PP trends and the timing of phytoplankton spring-summer bloom were observed in regions known for their great biological importance such as the coastal polynyas of northern Greenland.

## 1 Introduction

The impacts of environmental changes on Arctic and Sub-Arctic marine ecosystems are already detectable from field- (Grebmeier et al., 2006; Li et al., 2009) and satellite-based measurements (Arrigo and van Dijken, 2011; Arrigo et al., 2008; Kahru et al., 2011). While the overall increase in primary productivity (PP) has been attributed to a longer growing season, due to enhanced light availability for photosynthesis (Arrigo and van Dijken, 2011; Arrigo et al., 2008), changes in environmental forcing of nutrient supply to the surface have been proposed as the main driver of PP in seasonally ice-free waters (Tremblay and Gagnon, 2009).

At high northern latitudes, photosynthetically active radiation (PAR) is known to be an important limitation for marine photosynthesis. Environmental factors affecting the amount of PAR include cloud cover and the presence of sea ice and associated snow cover, which strongly attenuate

shortwave radiation. While the ice and snow cover have decreased significantly in recent decades (Comiso et al., 2008), cloud cover has increased (Eastman and Warren, 2010; Wang and Key, 2005). In fact, the shortwave radiation reaching the sea surface during summer months dropped at a mean annual rate of  $0.66 \text{ W m}^{-2} \text{ yr}^{-1}$  between 1982 and 1999 due to increasing cloudiness (Wang and Key, 2005). Climate models predict both a reduction in sea ice and an increase in cloud cover for the 21st century as the Arctic warms (Vavrus et al., 2010). During the open water season clouds typically cover 90 % of the sky, attenuating significantly the incoming shortwave radiation. Using satellite lidar measurements of cloud properties, Palm et al. (2010) found negative correlations between cloud fraction and sea ice coverage, suggesting that increasing temperature and moisture fluxes during ice-free period favors cloud formation. They also found greater low cloud frequency and cloud optical thickness above ice-free water areas (Palm et al., 2010). Although previous studies suggested that the Arctic region will become more productive overall due to a decline in the duration and extent of sea ice (Arrigo and van Dijken, 2011; Arrigo et al., 2008), the net effect of the opposing trends in the evolution of sea ice and cloud cover on PAR, and consequently on the marine primary productivity, has never been assessed.

The environmental forces that control vertical mixing in the upper ocean (e.g. wind, freshwater input) and, consequently the supply of nutrients to the sea surface, may counteract (increase stratification) (Li et al., 2009) or amplify (increased frequency of upwelling events that brings nutrient-rich waters to the surface) (Carmack and Chapman, 2003; Tremblay et al., 2011) the positive influence of increasing PAR. From the perspective of space-borne observation, a change in ocean stratification affecting nutrient supply should be detectable from the ensuing change in chlorophyll *a* concentration (CHL), a proxy for phytoplankton biomass routinely derived from remote sensing of ocean color (Behrenfeld et al., 2006).

Photosynthesis decreases when absorbing materials from terrestrial origin increase the blue light attenuation (Platt and Sathyendranath, 1993; Smyth et al., 2005). Shortly after the spring freshet, the Arctic shelves receive massive amounts of terrigenous colored dissolved organic matter (C-DOM) and suspended particulate material (SPM). The spread of terrigenous DOM over Arctic shelves in summer time can even be traced using spaceborne ocean color sensors (Fichot et al., 2013). Recent studies have reported increasing coastal erosion along several arctic coastline (Rachold et al., 2000) and river runoff at northern latitudes (Peterson et al., 2006). Models also predicted an important release of DOM into the Arctic Ocean (+700 %) from the carbon-rich Siberian peatlands (Frey and Smith, 2005). Diffuse attenuation coefficient of downward irradiance ( $K_d$ ) can, therefore, change due to variations in allochthonous material input. In contrast, removal processes of optically active constituents (e.g. CDOM photobleaching) can increase light penetration and favor PP. To de-

tect such changes in optically complex waters from space, PP models need to consider  $K_d$  independently from CHL (e.g. Smyth et al., 2005).

The objectives of this study were (1) to assess the trends in PAR reaching the sea surface vs. PAR penetrating the sea surface after considering sea ice cover, and (2) to quantify the relative contribution of changing PAR conditions due to sea ice, clouds and ocean optical properties, respectively, to the observed trends in PP. To achieve these objectives, we developed a PAR model that assimilates satellite-based cloud properties and a fully spectral PP model for optically complex Arctic waters. The implementation of the model was initiated as part of the Malina project in order to develop long-term monitoring capabilities of the Arctic's marine ecosystems productivity. We show that, over the 1998–2010 period of ocean color observation, PAR penetrating the ocean increased only slightly (but not significantly) in Arctic waters as a result of opposing trends in cloud and sea-ice cover. Nevertheless, a general positive PP trend was found and locally explained by concurrent changes in PAR, CHL and  $K_d$ , and the contribution of each factor varied strongly spatially.

## 2 Methods

### 2.1 PAR model

Space agencies distribute daily PAR as part as their ocean color databases, but areas partly covered by sea ice (a few percent of the area) are systematically discarded. Here we developed a method to assess incoming irradiance under all surface conditions in order to estimate PP in the vicinity of sea ice when ocean color data are available (see next section). Incident spectral downwelling irradiance at the sea surface,  $E_d(0+, \lambda, t)$ , was computed at 5 nm resolution every 3 h using a pre-computed look-up-table (LUT) generated using Santa Barbara DISORT Atmospheric Radiative Transfer model (SBDART, Ricchiazzi et al., 1998). The radiative transfer model inputs were: solar zenith angle ( $\theta_s$ ), total ozone concentration ( $O_3$ ), cloud fraction (CF) over the pixel and cloud optical thickness ( $\tau_{cl}$ ). The last three parameters were derived from satellite data (mainly AVHRR; Schweiger et al. 1999) following the method developed by Zhang et al. (2004) and were obtained from the International Satellite Cloud Climatology Project (ISCCP) web site. The ISCCP global radiative flux data (FD) are distributed on a 280 km equal-area grid at 3 h intervals for dates between January 1984 and December 2009.  $E_d(0+, \lambda, t)$  is calculated for each SeaWiFS 9 km pixel at a time interval of 3 h. The ISCCP products for each SeaWiFS pixel are obtained by bi-linear interpolation. When CF is not nil,  $E_d(0+, \lambda, t)$  is calculated for clear and cloudy (for the given  $\tau_{cl}$ ) sky conditions, respectively, and a weighed average is performed. Incident spectral downwelling irradiance just below the sea surface,  $E_d(0-, \lambda, t)$ , was calculated in the same way, but with a LUT for which

the air-to-sea interface reflection for both direct and diffuse components of the downwelling irradiance ( $\rho_{\text{Fresnel}}$ ) was accounted for. This correction assumes a  $\rho_{\text{Fresnel}}$  of 6.6% for the diffuse component of  $E_d$  (Morel, 1991) and the Fresnel's law in which  $\rho_{\text{Fresnel}}$  is a function of  $\theta_s$ . Here,  $\text{PAR}(0+)$  refers to the integral of  $E_d(0+, \lambda)$  from 400 to 700 nm (in  $\text{mol photon m}^{-2} \text{h}^{-1}$ ), while  $\text{PAR}(0-)$  is the integrated irradiance just below the sea surface ( $E_d(0-, \lambda)$ ) after considering the daily sea-ice concentration (SIC; in %) (i.e. multiply a factor of  $\cdot(1 - \text{SIC})$ ). Daily satellite-derived SIC data from the Defense Meteorological Satellite Program (DMSP) Scanning Multichannel Microwave Radiometer (SMMR), F8 and F13 Special Sensor Microwave Imager (SSM/I) (1984–2007) (Cavalieri et al., 1996) and F17 Special Sensor Microwave Imager/Sounder (SSMIS) (2008–2010) sensors (Maslanik and Stroeve, 1999) were obtained from the National Snow and Ice Data Center (NSIDC).

## 2.2 Primary production model

Daily PP rates were calculated using a common photosynthesis-irradiance model (i.e. P vs. I curve) proposed by Platt et al. (1980):

$$\text{PP} = \text{CHL} \cdot P_m^B \int_{t=0}^{24\text{h}} \int_{z=0.1\%}^{100\%} 1 - e^{-\frac{\text{PUR}(z,t)}{E_k}} dz dt \quad (1)$$

where chlorophyll *a* concentration (CHL; in  $\text{mg m}^{-3}$ ), photosynthetically usable radiation (PUR, in  $\text{mol photon m}^{-2} \text{s}^{-1}$ ), light-saturated CHL-normalized carbon fixation rate ( $P_m^B$ ; in  $\text{mg C (mg CHL)}^{-1} \text{h}^{-1}$ ), and saturation irradiance ( $E_k$ ,  $\text{mol photon m}^{-2} \text{s}^{-1}$ ) are needed for the calculation of PP at each depth. Ocean color data, binned at a 9.28 km resolution on an equal-area grid, were used for CHL and to calculate PUR at each depth in the water column. Briefly, monthly CHL data retrieved using a semi-analytical algorithm (GSM01) (Maritorena et al., 2002) were obtained from the Ocean Color MEaSUREs project (v6) at UCSB <http://wiki.icess.ucsb.edu/measures/Products>). GSM01 was found to perform better than standard empirical algorithms (e.g. NASA's OC4v6) in Arctic waters dominated by CDOM absorption (Ben Mustapha et al., 2012). Next, SeaWiFS Level 3 monthly water-leaving reflectance ( $R_{rs}$ ) at 412, 443, 490, 510, 555 and 670 nm were obtained from the NASA GSFC (reprocessing 2010.0). Spectral IOPs, namely the total absorption (*a*) and backscattering (*b<sub>b</sub>*) coefficients, were estimated from  $R_{rs}(\lambda)$  using a quasi-analytical algorithm (QAA) (Lee et al., 2002). The accuracy of the QAA in Arctic waters remains to be assessed, but a preliminary validation indicated an excellent performance of this algorithm for the retrievals of the total *a* and *b<sub>b</sub>* (absolute relative difference < 18%) (Bélanger, 2006). The in-water spectral diffuse attenuation coefficient  $K_d(\lambda)$  averaged over the euphotic zone was estimated following the approach of Lee et al. (2005)

using the QAA-derived IOPs as input.  $K_d(\lambda)$  was used to propagate  $E_d(z, \lambda, t)$  throughout the water column (Eq. 2). This was achieved at twelve optical depths from the sea surface to a level of 0.1% of the incident light.  $\text{PUR}(z, t)$  was calculated at each time step (3 h) and depth following Morel (1978):

$$\text{PUR}(z, t) = \int_{\lambda=400}^{700\text{nm}} E^0(\lambda, z, t) \cdot e^{-K_d(\lambda, t)z} \frac{a_{\text{ph}}(\lambda)}{a_{\text{ph}}(443)} d\lambda \quad (2)$$

where  $a_{\text{ph}}(\lambda)$  is the spectral phytoplankton absorption coefficient (in  $\text{m}^{-1}$ ), and  $E^0$  is the spectral scalar irradiance. The latter was calculated by dividing  $E_d$  by the mean cosine of downwelling irradiance (Morel, 1991), approximated by the expression  $\frac{(a+bb)}{K_d}$  (Sathyendranath et al., 1989).  $a_{\text{ph}}(\lambda)$  was calculated using an empirical statistical relationship established between  $a_{\text{ph}}(\lambda)$  and CHL derived from measurements made in the Western Arctic Ocean by Matsuoka et al. (2011).  $E_k$  decreased with depth due to photoacclimation, and varied as a function of mean daily PUR at each depth following Arrigo et al. (1998)'s model developed for high latitudes. Finally,  $P_m^B$  was assumed to be constant at  $2.0 \text{ mg C (mg CHL)}^{-1} \text{h}^{-1}$ , an averaged value based on field measurements in Arctic waters (Harrison and Platt, 1986; Huot et al., 2013).

The vertical attenuation of photosynthetically usable radiation,  $K_{\text{PUR}}$ , was calculated to express the variations in  $K_d(\lambda)$  using a single quantity meaningful with regards to primary production assessment (Platt and Sathyendranath, 1993).  $\text{PUR}(z)$  was calculated using Eq. (2), with given  $E^0(\lambda)$  for a clear sky with a sun zenith angle of  $60^\circ$ , allowing the estimation of the 1% light level for PUR ( $z_{1\% \text{ PUR}}$ ). Given that:

$$\text{PUR}(z) = \text{PUR}(0-) e^{-K_{\text{PUR}}z}, \quad (3)$$

$K_{\text{PUR}}$  was calculated as,

$$K_{\text{PUR}} = \frac{-4.6}{z_{1\% \text{ PUR}}}. \quad (4)$$

PP calculations were made at 3 h time interval, which corresponds to the ISCCP time resolution. Sea ice concentration was updated daily while IOPs and CHL were updated monthly. This procedure allowed calculations of PP under both cloudy and clear sky conditions, as long as IOPs and CHL were available. Here, gaps in the monthly fields of IOPs and CHL, which frequently occurred due to persistent cloud or sea-ice cover, were filled with monthly climatology of IOPs and CHL. Thus, when OC data were available, the PP was computed at 3 h interval for each day of the month. The daily PP rate of the pixel was adjusted as a function of the daily fraction of open water ( $1 - \text{SIC}$ ). PP was assumed nil where no IOPs and CHL data were available (i.e. pixels never documented by SeaWiFS). In other words, PP within open

waters that occurred in the central Arctic was not considered because ocean color data were unavailable. This method allowed us to consider the exact same surface area from year to year for the whole time series, and thereby minimizing the possible bias introduced by (1) the increasing number of ocean pixels documented by SeaWiFS through time as open-water area increases and (2) the extrapolation of PP rates in the area never observed from space-borne ocean color sensors.

### 2.3 Trends analysis

The trends in yearly PAR and PP over the 13 yr SeaWiFS time series were calculated for each pixel using a nonlinear trends estimator as described in Zhang et al. (2000). This is a non-parametric method that removes autocorrelation and outliers from the time series before calculating the trend using the Theil-Sen approach (TSA; Sen slope). The *zyp.zhang* function implemented in *R* was used. The Mann-Kendall non-parametric test was then run on the resulting time series to test the significance of the trends.

## 3 Results

### 3.1 Above-surface photosynthetically available radiation trends

Annual PAR reaching the sea surface (PAR(0+)) above the Arctic circle range from 3000 to 5500 mol photon $m^{-2}yr^{-1}$  (Fig. 1a). From 1998 to 2009, which corresponds approximately to the SeaWiFS era, PAR(0+) generally decreased at a rate ranging from  $-100$  to  $-50$  mol photon $m^{-2}yr^{-1}$  over seasonally and permanently open water (Fig. 1b), while it increased ( $\sim +50$  to  $+100$  mol photon $m^{-2}yr^{-1}$ ) in over the permanently ice-covered Central Arctic waters. The largest decrease in PAR(0+) were found between  $55^{\circ}N$  and  $70^{\circ}N$  (Hudson Bay, Gulf of Alaska, Bering Sea and Nordic Seas). Relative changes generally lay between  $\pm 2\%$   $yr^{-1}$  (Fig. 1c). Regionally integrated daily fluxes of PAR(0+) for each summer month are presented in Table 1 (see Fig. S1 for regional limits, Supplement). Significant negative trends ( $p < 0.05$ ) were observed in the Greenland, Barents, Kara, Laptev, East Siberian and Bering Seas at more than two months (Table 1). Above circum Arctic waters ( $\geq 66.58^{\circ}N$ ), annual PAR(0+) has decreased by  $\sim 10\%$  over the SeaWiFS era. PAR(0+) tended to decrease at all summer months with the largest relative rate occurring in June ( $-1.1\%$   $yr^{-1}$ ,  $p < 0.05$ ) when solar irradiance is maximum ( $\sim 39$  mol photon $m^{-2}d^{-1}$ , Table 1).

### 3.2 Below-surface photosynthetically available radiation trends

In the seasonally and permanently open water, sea ice is the primary factor controlling the penetration of PAR in the

ocean (Fig. 2a) (Perovich et al., 2007). There was a striking contrast in PAR(0-) trends between permanently ice-free waters and ice infested seas. As expected, PAR(0-) has increased significantly since 1998 at rates reaching up to  $+150$  mol photon $m^{-2}yr^{-1}$  at the margin of the Central ice pack (Fig. 2b) resulting in a relative increase of  $0.34\%$   $yr^{-1}$  in PAR for the circum-Arctic waters. Interestingly, the increase in the high Arctic ( $\geq 70^{\circ}N$ ) was largely counterbalanced by a general decrease in PAR(0-) between  $55$  to  $65^{\circ}N$  (Fig. 2b). Integrating total PAR(0-) over Arctic and sub-Arctic Seas (including Okhotsk Sea, Bering Sea, Labrador Sea and the Hudson Bay and Strait; see Fig. S1) resulted in slightly negative trend of  $-0.30\%$   $yr^{-1}$  (not significant). Regionally integrated daily fluxes of PAR(0-) for each summer month showed both positive and negative trends (Table 2). The largest positive trends in PAR(0-) was observed in the Beaufort Sea in June and July with values reaching as much as  $9.4\%$   $yr^{-1}$  and  $8.0\%$   $yr^{-1}$ , respectively, followed by the Kara Sea in May and June with  $5.0\%$   $yr^{-1}$  and  $4.4\%$   $yr^{-1}$ , respectively. Negative trends in PAR(0-) were found in the Atlantic sectors (Greenland Sea and Norwegian Sea) and Pacific sectors (Bering Sea, Gulf of Alaska).

### 3.3 Total circum-Arctic primary production

The PAR model was used to drive the primary production model as detailed in Sect. 2.2. Total circum-Arctic estimate of primary production was more than two fold smaller ( $203 \pm 15$  TgC  $yr^{-1}$ ) than previous satellite-based estimates (i.e.  $441$  to  $585$  TgC  $yr^{-1}$ ) (Arrigo et al., 2008; Arrigo and van Dijken, 2011). This result departure arises partly from the choices of ocean color algorithms and photosynthetic parameters used in the model. Our PP model explicitly accounts for the fact that Arctic waters are optically complex (Matsuoka et al., 2007; Siegel et al., 2005; Bélanger et al., 2008). Firstly, total light absorption and backscattering coefficients of seawater constituents were assessed from ocean color reflectance measurements to estimate the spectral diffuse attenuation (Lee et al., 2002, 2005). In general, PP models developed for clear case-1 waters employ empirical relationships between CHL and  $K_d$  or IOPs. We performed a sensitivity analysis, which compared our approach with three methods for  $K_d$ : (1) CHL vs. IOPs relationships from Wang et al. (2005)(W05); (2) CHL vs. IOPs relationships from Matsuoka et al. (2011) (MAT11); (3) CHL vs.  $K_d$  relationships established in case-1 waters by Morel and Maritorena (2001) (MM01). For the year 2007, the annual circum-Arctic PP obtained were  $60\%$ ,  $42\%$  and  $82\%$  higher than our estimate for W05, MAT11 and MM01 methods, respectively. Secondly, CHL was retrieved using a semi-analytical approach that minimize the effect of colored detrital matter (CDM), which is dominant in the Arctic (Bélanger et al., 2008; Matsuoka et al., 2007, 2011; Wang et al., 2005). Again, a calculation using the standard NASA algorithm (i.e. OC4), yield an annual PP  $\sim 7\%$  higher than the GSM algorithm. Interestingly, when PP is

**Table 1.** Regionally averaged daily flux of PAR above the sea (ice) surface (PAR(0+) in mol photon m<sup>-2</sup> d<sup>-1</sup>) and its relative trends computed for the 1998 to 2009 period (in parenthesis, in % yr<sup>-1</sup>). Significant trends are in bold text with superscript indicating the level of significance: (a) 0.05 < *p* < 0.1, (b) 0.01 < *p* < 0.05 and (c) *p* < 0.01

Region	May	June	July	August	September
Greenland Sea	29.0 ( <b>-0.90</b> ) <sup>a</sup>	38.6 ( <b>-1.07</b> ) <sup>c</sup>	34.6 (-0.52)	22.4 ( <b>-0.98</b> ) <sup>c</sup>	14.8 (-0.37)
Norwegian Sea	33.3 (-0.20)	37.8 (-0.42)	33.5 ( <b>-1.16</b> ) <sup>c</sup>	24.2 (-0.71)	12.8 ( <b>-0.88</b> ) <sup>c</sup>
Barents Sea	28.0 ( <b>-1.06</b> ) <sup>b</sup>	37.1 ( <b>-1.86</b> ) <sup>c</sup>	33.9 (-0.83)	21.0 ( <b>-0.93</b> ) <sup>b</sup>	13.3 ( <b>-1.15</b> ) <sup>c</sup>
Kara Sea	24.6 (-0.64)	35.6 ( <b>-0.94</b> ) <sup>b</sup>	35.3 (-0.67)	22.2 ( <b>-1.41</b> ) <sup>c</sup>	17.4 ( <b>-1.35</b> ) <sup>b</sup>
Laptev Sea	26.3 (-0.44)	35.7 ( <b>-1.54</b> ) <sup>b</sup>	35.8 ( <b>-1.29</b> ) <sup>b</sup>	22.7 ( <b>-0.95</b> ) <sup>b</sup>	17.6 ( <b>-0.85</b> ) <sup>c</sup>
East Siberian Sea	28.0 ( <b>-1.53</b> ) <sup>a</sup>	41.2 (-0.72)	39.8 ( <b>-0.98</b> ) <sup>b</sup>	25.1 ( <b>-0.79</b> ) <sup>a</sup>	17.3 ( <b>-0.84</b> ) <sup>b</sup>
Chukchi Sea	33.0 (-0.72)	46.0 (-0.93)	40.9 (-0.98)	26.3 (0.12)	12.8 (-0.51)
Beaufort Sea	29.9 ( <b>-1.86</b> ) <sup>b</sup>	44.9 (-0.40)	42.2 (-0.02)	27.5 (-0.20)	18.6 (-0.52)
Arctic Ocean	26.1 (-0.85)	36.9 (-0.92)	38.2 (-0.45)	23.5 (-0.21)	21.1 (0.24)
Northwestern Passages	29.5 (-0.63)	40.8 (-0.34)	40.8 (-0.38)	25.9 (-0.32)	14.8 (-0.26)
Baffin Bay	29.2 (-0.41)	40.0 ( <b>-0.95</b> ) <sup>b</sup>	37.8 (0.39)	23.2 (0.24)	11.0 (-0.21)
Hudson Bay	34.2 ( <b>-1.65</b> ) <sup>c</sup>	46.0 ( <b>-0.64</b> ) <sup>a</sup>	46.1 (-0.28)	33.3 (-0.53)	18.8 (-0.26)
Hudson Strait	31.9 (-0.87)	41.8 (-0.03)	43.9 (-0.35)	30.4 (-0.34)	17.6 (-0.69)
Davis Strait	33.4 ( <b>-0.68</b> ) <sup>c</sup>	41.1 (-0.44)	40.7 (-0.03)	28.1 ( <b>-0.70</b> ) <sup>b</sup>	15.8 (-0.88)
Labrador Sea	36.5 (-0.47)	40.3 (-0.23)	39.5 (-0.22)	31.1 ( <b>-0.65</b> ) <sup>b</sup>	20.7 (-0.18)
Sea of Okhotsk	37.9 ( <b>-0.60</b> ) <sup>b</sup>	43.0 (0.27)	39.9 (-1.03)	31.2 (-0.62)	22.3 (-0.14)
Bering Sea	34.6 ( <b>-0.99</b> ) <sup>b</sup>	37.0 ( <b>-1.0</b> ) <sup>c</sup>	34.5 ( <b>-0.98</b> ) <sup>b</sup>	27.1 (-0.79)	18.7 ( <b>-0.87</b> ) <sup>c</sup>
Gulf of Alaska	38.5 ( <b>-1.06</b> ) <sup>b</sup>	41.3 (-0.39)	37.6 (-0.67)	31.2 ( <b>-1.15</b> ) <sup>a</sup>	19.7 (-0.74)
<b>Arctic + sub-Arctic Seas</b>	<b>33.0 (-0.86)</b> <sup>b</sup>	<b>39.6 (-0.71)</b> <sup>c</sup>	<b>37.4 (-0.84)</b> <sup>c</sup>	<b>26.0 (-0.57)</b> <sup>c</sup>	<b>17.1 (-0.67)</b> <sup>c</sup>
<b>Circum Arctic</b>	<b>29.2 (-0.71)</b>	<b>38.7 (-1.11)</b> <sup>b</sup>	<b>36.4 (-0.63)</b>	<b>23.3 (-0.31)</b>	<b>15.6 (-0.48)</b> <sup>b</sup>

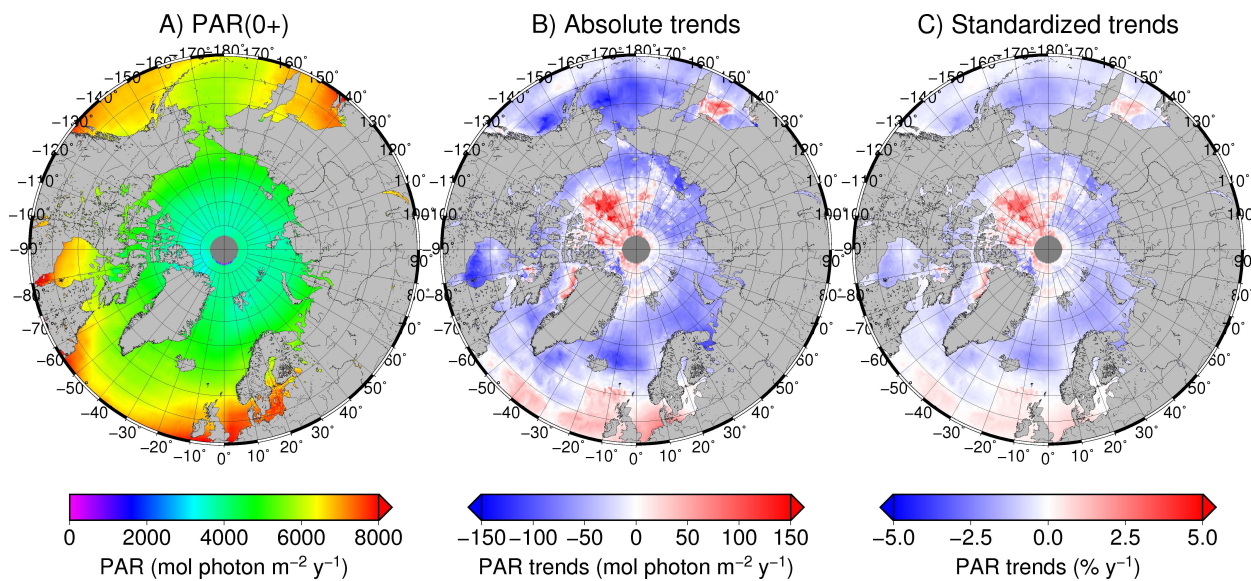


**Fig. 1.** (A) Mean yearly downwelling flux of PAR above the sea (ice) surface (PAR(0+)) for the 1998 to 2009 period, (B) Absolute PAR(0+) trends calculated using the TSA, and (C) the standardized PAR(0+) trends (i.e. PAR(0+) trends/climatological PAR(0+) · 100).

calculated using CHL from OC4 and  $K_d$  from W05, the total PP rises by  $\sim 85\%$  to reach  $357 \pm 15 \text{ TgC yr}^{-1}$ , which is still lower than previous estimation of Arrigo et al. (2008). Thirdly, the spectral shape of phytoplankton absorption coefficient is given by statistical relationships published by Matsuoka et al. (2011). The case-1 waters parameterization of

Bricaud et al. (1998) yields an annual PP 12% higher than our estimation. Finally, the light-saturated CHL-normalized carbon fixation rate,  $P_m^B$ , which usually varies as a function of sea surface temperature in PP models, is fixed to a constant in our model ( $2.0 \text{ mg C (mg CHL)}^{-1} \text{ h}^{-1}$ ) due to a lack of robust parameterization for arctic waters (Huot et al., 2013).

**Table 2.** Regionally averaged daily flux of PAR just beneath the sea surface (PAR(0–) in mol photon m<sup>-2</sup> d<sup>-1</sup>) and its relative trends computed for the 1998 to 2009 period (in parenthesis, in % yr<sup>-1</sup>). Significant trends are in bold text with superscript indicating the level of significance: (a) 0.05 < p < 0.1, (b) 0.01 < p < 0.05, and (c) p < 0.01

Region	May	June	July	August	September
Greenland Sea	22.5 (–0.46)	27.9 (– <b>1.16</b> ) <sup>c</sup>	26.9 (– <b>0.86</b> ) <sup>c</sup>	18.3 (– <b>1.01</b> ) <sup>b</sup>	11.5 (–0.93)
Norwegian Sea	30.3 (–0.18)	33.3 (–0.42)	30.5 (– <b>1.16</b> ) <sup>c</sup>	22.0 (–0.71)	11.6 (– <b>0.88</b> ) <sup>c</sup>
Barents Sea	19.4 (2.09)	27.4 (0.19)	28.9 (–0.94)	18.7 (– <b>0.76</b> ) <sup>b</sup>	11.7 (–0.61)
Kara Sea	4.2 ( <b>5.03</b> ) <sup>c</sup>	10.8 ( <b>4.41</b> ) <sup>b</sup>	20.3 ( <b>2.48</b> ) <sup>a</sup>	16.9 (0.40)	12.9 (0.67)
Laptev Sea	5.4 (1.90)	12.3 (1.14)	18.6 (0.66)	16.8 (–1.02)	12.7 (–0.98)
East Siberian Sea	3.3 (4.05)	9.7 (2.13)	17.9 (1.71)	17.9 (1.10)	12.4 (1.33)
Chukchi Sea	8.1 (1.74)	21.6 (2.55)	31.9 (0.74)	23.1 (0.25)	11.4 (–0.05)
Beaufort Sea	4.7 (1.19)	14.3 ( <b>9.35</b> ) <sup>b</sup>	21.2 ( <b>8.01</b> ) <sup>c</sup>	17.5 ( <b>3.34</b> ) <sup>a</sup>	11.2 (3.97)
Arctic Ocean	5.6 (3.52)	8.3 (6.91)	14.0 ( <b>4.38</b> ) <sup>c</sup>	12.7 ( <b>3.36</b> ) <sup>b</sup>	10.9 ( <b>3.03</b> ) <sup>b</sup>
Northwestern Passages	6.3 (2.11)	15.4 ( <b>3.99</b> ) <sup>b</sup>	20.2 ( <b>2.13</b> ) <sup>a</sup>	17.6 (1.83)	10.3 (1.05)
Baffin Bay	10.6 (3.82)	19.9 (1.91)	28.6 (0.61)	20.1 (0.56)	9.3 (0.18)
Hudson Bay	10.0 (–2.57)	21.9 (–3.16)	38.4 (–0.32)	29.7 (–0.48)	16.8 (–0.16)
Hudson Strait	10.1 (–0.42)	24.6 (–0.13)	38.5 (–0.18)	27.2 (–0.31)	15.8 (–0.51)
Davis Strait	24.5 (0.24)	30.3 (–0.27)	34.0 (0.22)	25.1 (–0.48)	14.2 (–0.88)
Labrador Sea	30.6 (–0.52)	34.6 (–0.29)	35.8 (–0.22)	28.2 (– <b>0.65</b> ) <sup>b</sup>	18.7 (–0.15)
Sea of Okhotsk	30.8 (–0.34)	36.7 (0.19)	36.2 (– <b>1.10</b> ) <sup>a</sup>	28.3 (–0.63)	20.2 (–0.15)
Bering Sea	29.1 (–1.19)	32.2 (– <b>0.98</b> ) <sup>b</sup>	31.3 (– <b>0.98</b> ) <sup>b</sup>	24.6 (–0.79)	16.9 (– <b>0.86</b> ) <sup>c</sup>
Gulf of Alaska	34.5 (–0.72)	36.3 (–0.39)	34.2 (–0.67)	28.3 (– <b>1.15</b> ) <sup>a</sup>	17.9 (–0.74)
<b>Arctic + sub-Arctic Seas</b>	24.6 (–0.27)	27.7 (–0.12)	28.9 (–0.15)	21.7 (–0.18)	13.9 (–0.10)
<b>Circum Arctic</b>	18.5 (0.37)	22.6 (0.16)	24.2 (0.49)	17.8 (0.42)	11.4 (0.43)

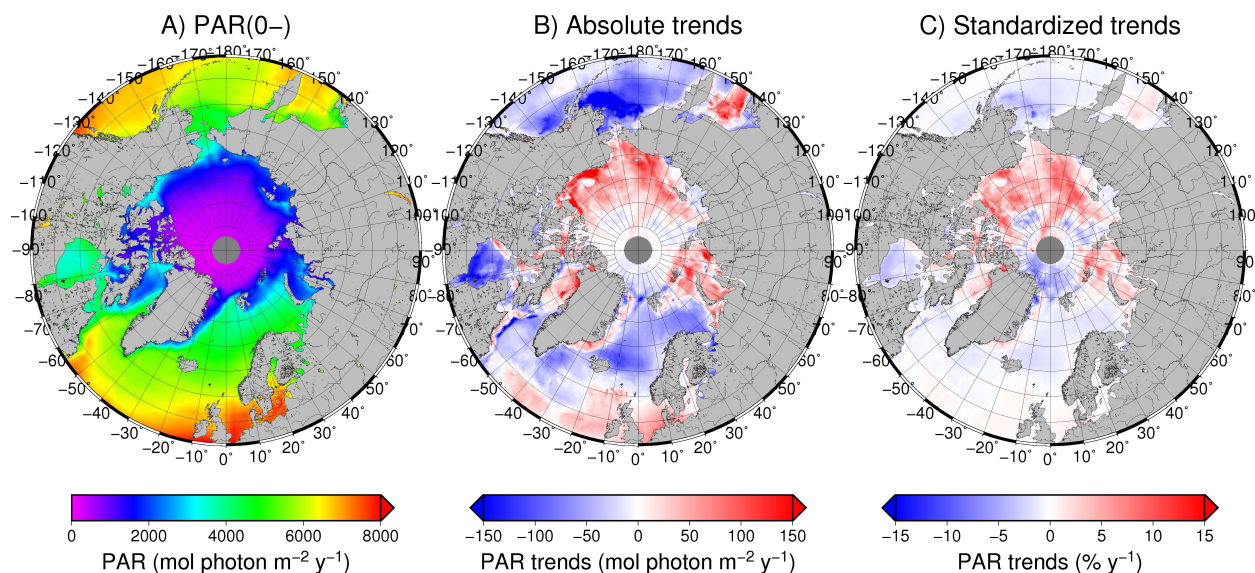


**Fig. 2.** Same as Fig. 1, but for PAR just below the air-sea interface (PAR(0–)).

### 3.4 Primary production trends

Figure 3b shows that PP changes are spatially heterogeneous and relatively small over most of the circum Arctic Ocean ( $\leq 3 \text{ gC m}^{-2} \text{ yr}^{-1}$ ). The overall positive trend in PP is mostly driven by the historically productive regions of inflow (Barents and Chukchi) and interior (e.g. Kara, Laptev,

East Siberian and Beaufort Seas) shelves (Fig. 3b). Because small relative changes in these productive areas can dwarf large relative changes in unproductive areas, the standardized trends presented in Fig. 3c provide a better assessment of intra-regional changes than do absolute trends. After standardization, positive trends are found on seasonally ice-free inflow and interior shelves, as well as in permanently open

waters (Southern Iceland Shelf, Western Bering Sea). Negative trends are found along major exit routes of Arctic waters over outflow shelves in the Eastern Greenland Sea and Canadian Archipelago (e.g. northwestern Baffin Bay, Lancaster Sound), and in the northern part of the Bering Sea.

PP integrated over the circum-Arctic increased for each summer months and the trend was significant in May, June, August and September (Table 3). The largest increase in PP occurred during the month of May (+0.85 TgCyr<sup>-1</sup> or +2.38 % yr<sup>-1</sup>) followed by June (+0.65 TgCyr<sup>-1</sup> or +1.60 % yr<sup>-1</sup>) (Table 3). The Barents Sea is the area where the increase was the most pronounced in May (+3.1 % yr<sup>-1</sup>, 14.6 mg C m<sup>-2</sup> d<sup>-1</sup> yr<sup>-1</sup>), while the northern Barents Sea and the southeastern Beaufort Sea showed the highest increase in June (+15.3 % yr<sup>-1</sup>, 21 mg C m<sup>-2</sup> d<sup>-1</sup> yr<sup>-1</sup>). A similar seasonal pattern in PP trends, though with smaller relative changes (~ +1 % yr<sup>-1</sup>), were found when considering both Arctic and sub-Arctic Seas (Table 3).

### 3.5 Trends in ocean optical properties

The above results show that changes in PAR(0–) alone only partly explain the general increase in PP (Figs. 2 vs. 3). This was expected since PP is, to the first order, strongly dependent on phytoplankton biomass (CHL) and, to a lesser extent, to PAR and diffuse light attenuation. We, therefore, examined how ocean optical properties (i.e. CHL and K<sub>PUR</sub>) have changed between 1998 to 2010. Here the changes in the ratio of CHL and K<sub>PUR</sub> (CHL/K<sub>PUR</sub>), a quantity directly proportional to depth-integrated PP, are analysed. This choice is inspired from Platt and Sathyendranath (1993), who demonstrated, using a dimensional analysis, that PP models commonly used in Ocean Color remote sensing can be expressed using a simple canonical form,

$$PP = \frac{P_m^B \cdot CHL \cdot D}{K_{PAR}} \cdot f(PAR(0-)_m^*) \quad (5)$$

where D is the day length, K<sub>PAR</sub> is the diffuse attenuation of PAR and  $f(PAR(0-)_m^*)$  is a dimensionless factor that depends on the mid-day PAR(0–) normalised to E<sub>K</sub>.  $f(PAR(0-)_m^*)$  depends on the model choice for P vs. I curve (Eq. 1), the magnitude of incident PAR and the function chosen to describe the variation of surface irradiance through the day. The factor  $\frac{P_m^B \cdot CHL \cdot D}{K_{PAR}}$  is common to most satellite-based models that assumes vertically homogenous CHL profiles (Platt and Sathyendranath, 1993). This dependency can be demonstrated analytically by integrating Eq. (1) with a few assumptions (see Supplement for details). In most satellite-based approaches, however, K<sub>PAR</sub> is a function CHL, rendering the evaluation of CHL/K<sub>PAR</sub> irrelevant. In our case, K<sub>PUR</sub> is used instead of K<sub>PAR</sub> to better take into account for spectral effect of light attenuation and the phytoplankton spectral absorption properties. More importantly, K<sub>PUR</sub> is not fully dependent on CHL because it was assessed using the QAA algorithm. Thus, in the context of a PP trends analysis with

our approach, trends in ocean optical properties are best represented by CHL/K<sub>PUR</sub>.

Figure 4 illustrates the relationships between satellite-derived products and their relation to PP. In the open ocean, the variability in K<sub>PUR</sub> is largely controlled by phytoplankton biomass. In July 2007, for example, 82 % of the variance in K<sub>PUR</sub> in the circum-Arctic was explained by CHL (Fig. 4a). The remaining variance (18 %) was due to other optically significant constituents, or phytoplankton pigments characteristics that influence K<sub>PUR</sub>. It also shows that the K<sub>PUR</sub> for a given value of CHL is much higher than the value predicted the case-1 water model published by Morel and Maritorena (2001). The differences are more pronounced in the low chlorophyll *a* concentration range and tend to diminish as CHL increases. Consequently, PP will be lower in the Arctic for a given CHL concentration as compared to the open ocean.

When PP is normalized to the incident irradiance (PAR(0–)), denoted as PP\*, a strong positive relationship was obtained with CHL ( $r^2 = 0.92$ ; Fig. 4b). Note that PAR(0–) alone explained 18 % of the variance in PP (not shown). Similarly, PP\* was also positively correlated to K<sub>PUR</sub> due to its dependence on CHL ( $r^2 = 0.58$ ; Fig. 4c). Figure 4d shows the strong relationship existing between PP\* and the ratio of CHL/K<sub>PUR</sub> ( $r^2 = 0.98$ ). This result was expected (Eq. 5) since the light-saturated CHL-normalized carbon fixation rate was set to a constant value. Note that the remaining variability on Fig. 5d is due to the model choice for P vs. I curve (Eq. 1) and the parameterization of E<sub>K</sub> (i.e.,  $f(PAR(0-)_m^*)$  in Eq. 5).

The seasonal variation in CHL/K<sub>PUR</sub> is shown on Fig. 5a–d, where a general decrease is observed from May to August. Most Arctic waters exhibited CHL/K<sub>PUR</sub> < 2.5 mgCHL m<sup>-2</sup>, which is lower than the averaged values found in the North Atlantic and North Pacific (> 3 mgCHL m<sup>-2</sup>). In May, relatively high values were found in sectors known to host intense spring phytoplankton blooms, such as the Barents and Chukchi Seas and the Baffin Bay (North Water (NOW), West Greenland Current (WGC) (Fig. 5a; Table 4). In contrast, CHL/K<sub>PUR</sub> remained low during the whole summer season in strongly stratified arctic waters (e.g. Canada Basin < 1 mgCHL m<sup>-2</sup>). In August, most arctic waters are strongly stratified except in regions where deep-water upwellings are dominant (e.g. northeast Greenland, Hudson Strait, Siberian coastal waters) (Fig. 5d). At the regional scale, the highest CHL/K<sub>PUR</sub> values were observed in the Laptev Sea in summer (> 9 mgCHL m<sup>-2</sup>, Table 4), which are likely too high in these waters heavily influenced by large Siberian river inputs of CDOM and detrital material (Fichot et al., 2013).

The monthly trends depicted in Fig. 5e–l, showed a general increase of CHL/K<sub>PUR</sub> in May, particularly in the southern Labrador Sea, northern Baffin Bay (i.e. the NOW), the southern portion of the East Greenland Current (EGC) and southern Barents Sea. In June, the positive trends were found in

**Table 3.** Regionally averaged daily flux of PP (in mg C m<sup>-2</sup> d<sup>-1</sup>) and its relative trends computed for the 1998 to 2010 period (in parenthesis, in % yr<sup>-1</sup>). Significant trends are in bold text with superscript indicating the level of significance: (a) 0.05 < *p* < 0.1, (b) 0.01 < *p* < 0.05, and (c) *p* < 0.01

Region	May	June	July	August	September
Greenland Sea	263 (2.36)	352 (0.63)	193 (−0.56)	111 (0.14)	86 (0.62)
Norwegian Sea	273 (1.82)	314 (0.42)	224 (−0.05)	167 (0.76)	111 (−0.07)
Barents Sea	467 ( <b>3.13</b> <sup>a</sup> )	233 (2.08)	168 ( <b>1.44</b> <sup>b</sup> )	123 ( <b>1.43</b> <sup>b</sup> )	93 (0.56)
Kara Sea	49 ( <b>4.61</b> <sup>c</sup> )	221 ( <b>4.26</b> <sup>b</sup> )	358 ( <b>2.61</b> <sup>c</sup> )	369 (−0.14)	311 (0.35)
Laptev Sea	122 (2.20)	220 (1.99)	505 (1.85)	527 (0.88)	410 (0.08)
East Siberian Sea	42 (5.00)	147 (4.14)	351 (2.06)	316 ( <b>2.21</b> <sup>a</sup> )	222 ( <b>2.25</b> <sup>a</sup> )
Chukchi Sea	128 (0.99)	224 (4.70)	184 (1.74)	151 (2.67)	112 ( <b>0.86</b> <sup>b</sup> )
Beaufort Sea	47 (0.39)	140 ( <b>15.3</b> <sup>b</sup> )	211 ( <b>3.38</b> <sup>b</sup> )	160 (−0.41)	96 (0.98)
Arctic Ocean	105 (5.19)	92 ( <b>8.77</b> <sup>a</sup> )	82 ( <b>4.57</b> <sup>c</sup> )	80 ( <b>4.11</b> <sup>b</sup> )	75 ( <b>3.74</b> <sup>b</sup> )
Northwestern Passages	53 (3.41)	95 ( <b>4.10</b> <sup>b</sup> )	111 (0.62)	95 (1.78)	64 (3.08)
Baffin Bay	163 ( <b>5.06</b> <sup>b</sup> )	172 (0.35)	148 (−1.04)	98 ( <b>4.88</b> <sup>b</sup> )	65 (2.42)
Hudson Bay	93 (−2.08)	154 (0.37)	194 ( <b>2.15</b> <sup>b</sup> )	164 ( <b>2.05</b> <sup>b</sup> )	128 ( <b>1.06</b> <sup>b</sup> )
Hudson Strait	60 (1.75)	198 (0.36)	240 (−0.46)	150 (−0.07)	103 (0.41)
Davis Strait	309 (0.78)	168 (0.94)	178 (0.91)	121 (0.15)	86 (1.04)
Labrador Sea	231 (1.99)	287 (0.71)	211 (0.98)	130 (−0.34)	98 ( <b>1.93</b> <sup>b</sup> )
Sea of Okhotsk	383 ( <b>2.86</b> <sup>b</sup> )	444 (1.52)	240 (0.67)	171 (3.07)	135 ( <b>2.04</b> <sup>b</sup> )
Bering Sea	343 (1.14)	345 ( <b>2.94</b> <sup>b</sup> )	225 (−0.66)	196 (0.96)	154 ( <b>1.18</b> <sup>a</sup> )
Gulf of Alaska	384 (1.60)	335 (−0.38)	254 (0.68)	221 ( <b>2.76</b> <sup>b</sup> )	171 (0.75)
<b>Arctic + sub-Arctic Seas</b>	<b>302 (1.49)<sup>b</sup></b>	280 (1.32)	222 ( <b>0.74</b> <sup>a</sup> )	177 ( <b>1.21</b> <sup>c</sup> )	135 ( <b>0.96</b> <sup>c</sup> )
<b>Circum Arctic</b>	<b>276 (2.38)<sup>c</sup></b>	237 ( <b>1.60</b> <sup>a</sup> )	214 (0.92)	175 ( <b>1.08</b> <sup>b</sup> )	133 ( <b>0.83</b> <sup>a</sup> )

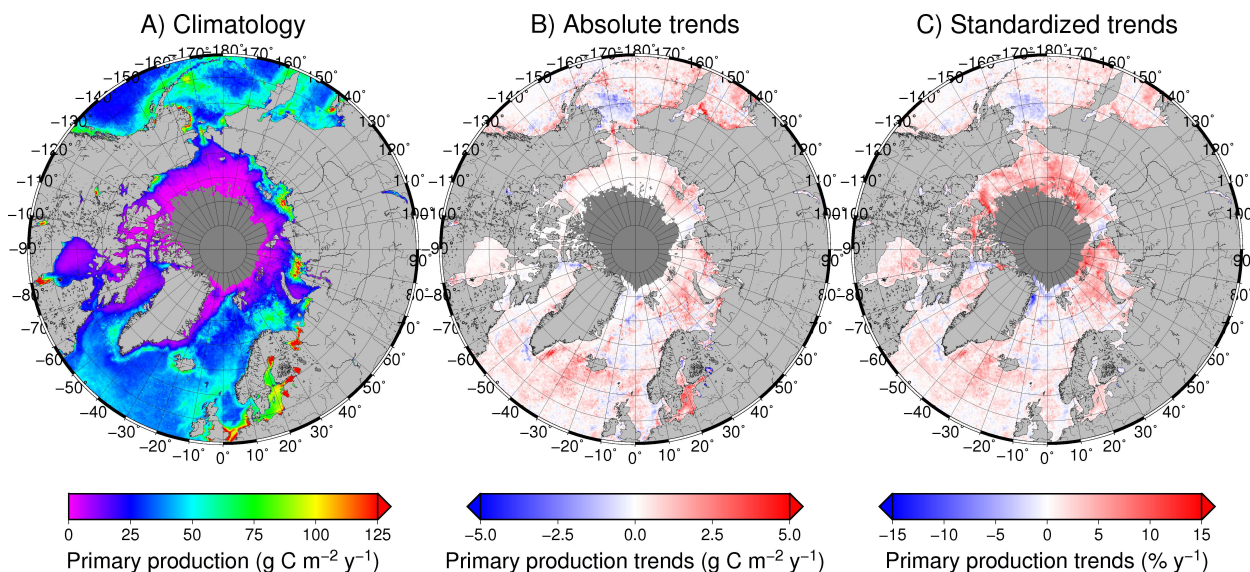


**Fig. 3.** (A) Climatological primary production rates for the 13 yr SeaWiFS time series (1998–2010), (B) Absolute PP trends calculated using the TSA, and (C) the standardized PP trends (i.e. PP trends/climatological PP · 100).

the northern Labrador, northern Barents and southern Bering Seas, and negative trends in the northern Baffin Bay and northern Bering Sea (Fig. 5f, j). In July, positive trends are found in the Hudson Bay, the southern part of the WGC and the southern Barents and Chukchi Seas (Fig. 5g, k), whereas relatively strong negative trends occurred in coastal waters of

northern Greenland (both EGC and WGC) and in the Northwestern Passages (Table 4). In August, a positive trend remains in the Hudson Bay, the Chukchi and Barents Seas, and the central Baffin Bay (Fig. 5l), but the absolute trends were small, excepted in the Bering Strait and the Laptev Sea

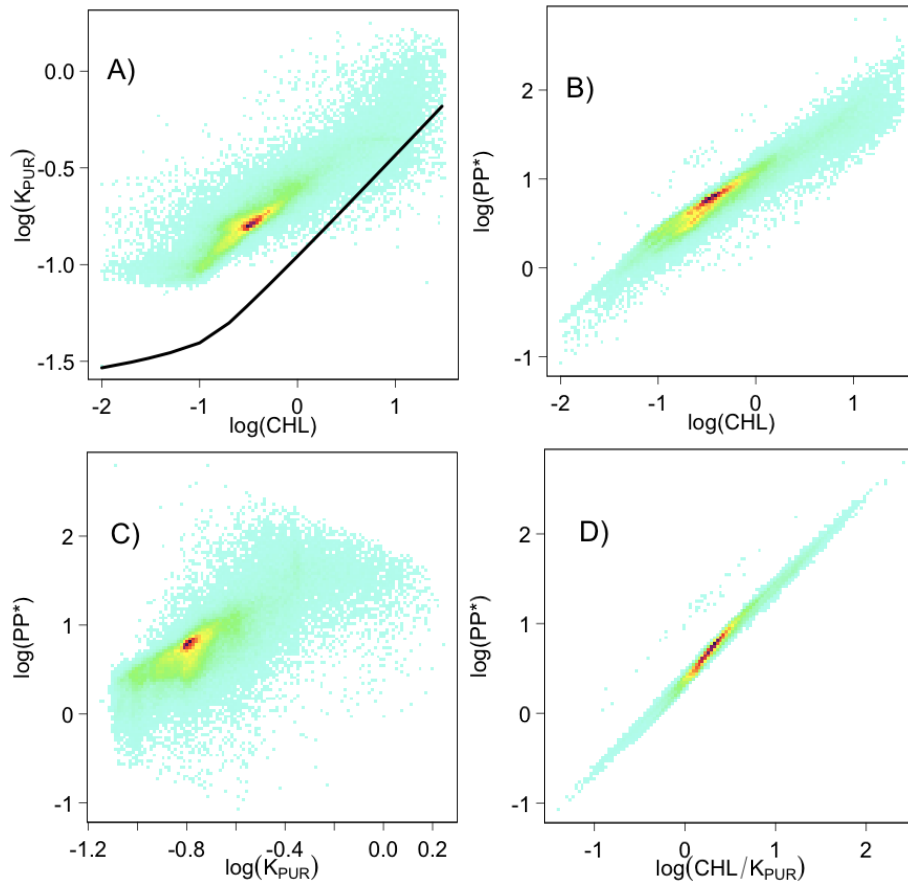


**Fig. 4.** Examples of relationship between (A) CHL and  $K_{\text{PUR}}$ , (B) CHL and PP normalized by surface PAR ( $\text{PP}^*$ ), (C)  $K_{\text{PUR}}$  and  $\text{PP}^*$ , and (D)  $\text{CHL}/K_{\text{PUR}}$  and  $\text{PP}^*$  for the month of July 2007. The black line on panel (A) is  $K_{\text{PUR}}$  predicted from CHL using the empirical model of Morel and Maritorena (2001) for  $K_d$  and Matsuoka et al. (2011) for  $a_{\text{ph}}$ .

(Fig. 5h). Again, significantly negative trends were observed in the Northwestern Passages ( $-1\%$ ,  $p < 0.05$ ; Table 4).

At the pan-Arctic scale,  $\text{CHL}/K_{\text{PUR}}$  did not vary significantly when the data above the Arctic Circle were pooled together, but significant positive trends were obtained in May, June, August and September when sub-Arctic Seas were considered (Table 4).

#### 4 Discussion and conclusions

The decrease in  $\text{PAR}(0+)$  over open water was nearly ubiquitous between  $55^\circ\text{N}$  and  $70^\circ\text{N}$ , with decadal reduction of 8% for the integrated circum-Arctic and sub-Arctic Seas and up to 20% in specific areas (e.g. Barents Sea in June, Table 1). This trend is consistent with several studies reporting strong positive anomalies in cloud amount above newly opened waters during summer and early fall (Eastman and Warren, 2010; Vavrus et al., 2010; Palm et al., 2010; Wang and Key, 2005). Increased cloudiness thus partly counteracts the positive influence of declining sea ice on  $\text{PAR}(0-)$  and renders the change in  $\text{PAR}(0-)$  non-significant over the 13 yr

study period (Table 2;  $+3.4\%$  per decade in the circum Arctic and  $-3\%$  over both Arctic and sub-Arctic Seas; Fig. 3). Warmer temperature and moisture fluxes are likely the main drivers of the increase in cloudiness (Eastman and Warren, 2010; Vavrus et al., 2010; Palm et al., 2010; Wang and Key, 2005). The positive trends over the perennially ice-covered ocean is, however, more uncertain due to the lower quality of cloud properties retrievals over ice covered conditions (Schweiger et al., 1999; Chernokulsky and Mokhov, 2012).

Depending on region, the light attenuation due to the cloud cover potentially reduced the total annual PP from  $\sim 18\%$  in the Canadian archipelago (Northwestern Passages, Hudson Strait) to up to 32% over the Siberian shelves (Laptev and Kara Seas) (Table 5). These numbers were obtained by assuming an hypothetically cloud-free atmosphere all year round ( $\text{PP}^{\text{clear sky}}$ ), which would obviously have strong impacts on the ocean heat budget, mixing and stratification, therefore modifying the supply of nutrients in the euphotic zone and the total PP. It is nevertheless a good way to assess the potential damping of PP due to cloud cover. Figure 6 and Table 5 show the trends of the potential reduction of the total

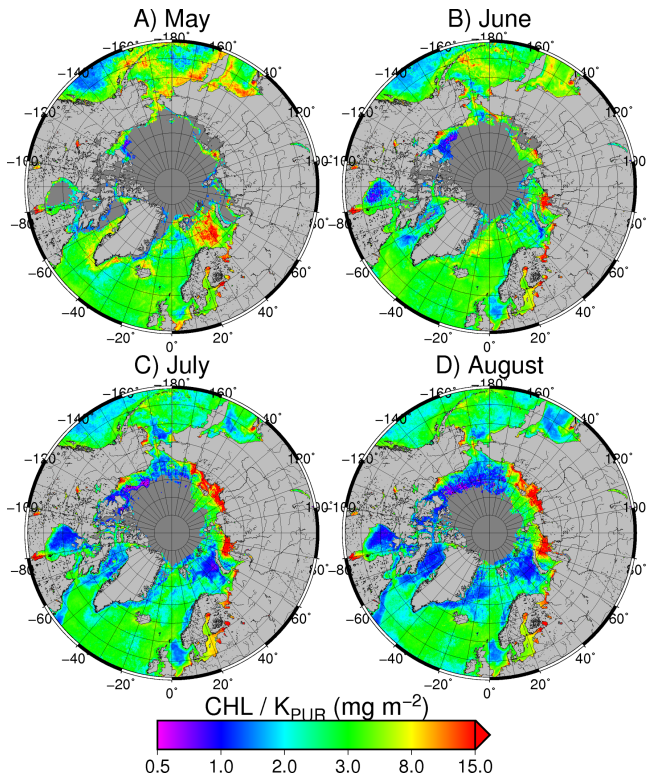


**Fig. 5.** (A–D) Monthly climatology of the ratio between CHL and the diffuse attenuation of PUR ( $CHL/K_{PUR}$ ); (E–H) absolute  $CHL/K_{PUR}$  trends calculated using the TSA, and (I–L) the standardized  $CHL/K_{PUR}$  trends (i.e.  $CHL/K_{PUR}$  trends/climatological  $CHL/K_{PUR} \cdot 100$ ).

annual PP due to cloudiness. At the pan-Arctic scale, the increasing cloudiness damps the total annual PP by  $\sim 3.5\%$  per decade. The trend is particularly important over the Eurasian part of the Arctic with a maximum value of  $5.3\%$  decade $^{-1}$  observed in the Barents Sea (Table 5).

Previous analyses of satellite-based PP time series revealed significant variability in spatial patterns and temporal trends across Arctic marine ecosystems (Arrigo and van Dijken, 2011; Arrigo et al., 2008; Kahru et al., 2011; Perrette et al., 2011). Here we also found a significant ( $p < 0.05$ ) PP trend of  $+2.8 \text{ TgCyr}^{-1}$  (or  $+1.4\%$  yr $^{-1}$  in relative terms) between 1998 and 2010 for the circum-Arctic. Longer growing season and light availability (i.e. PAR(0–)) was previously identified as a main driver of change in the high Arctic (Arrigo and van Dijken, 2011; Arrigo et al., 2008). We also found a correlation between annual PAR and PP anomalies across the circum-Arctic ( $r^2 = 0.42$ ,  $p < 0.001$ ; not shown). However, changes in light availability do not alone explain the positive PP trends in many Arctic sectors, except on Arctic interior shelves where PAR(0–) is largely driven by SIC (Figs. 2 vs. 3). In many regions, such as Hudson Bay, Baffin Strait, Baffin Bay and the Labrador, Norwegian and Barents Seas, PAR(0–) decreased while PP increased. The pattern in

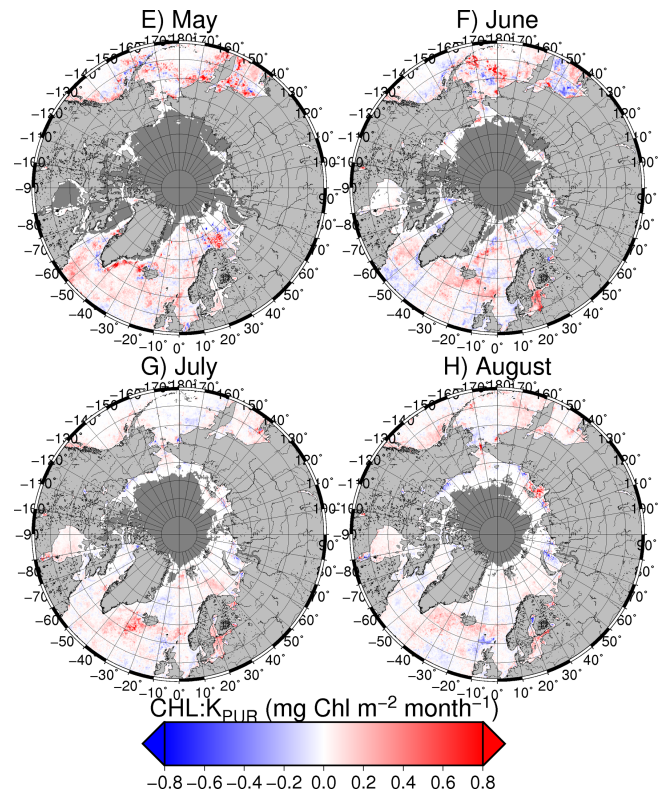


**Fig. 5.** Continued.

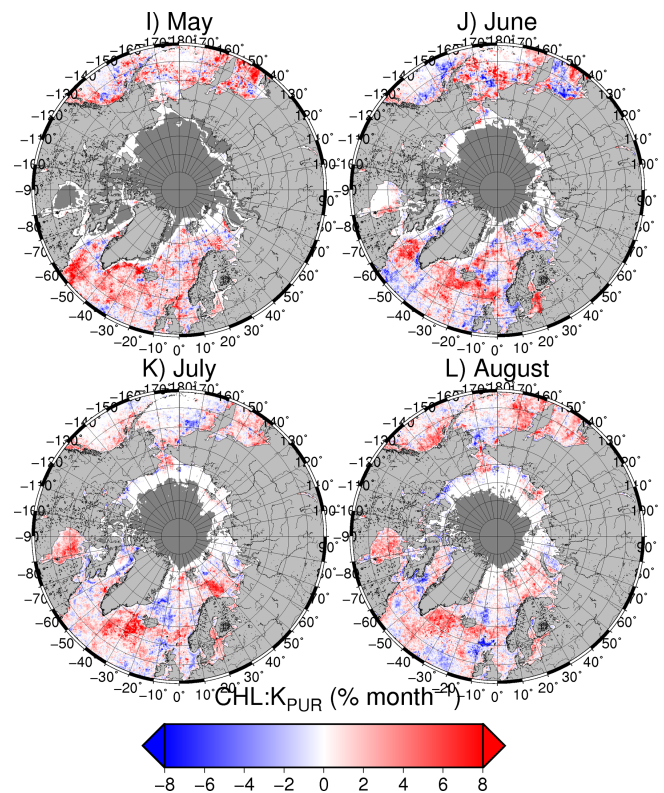


**Fig. 5.** Continued.

**Table 4.** Regionally averaged CHL/ $K_{PUR}$  (in mg CHL  $m^{-2}$ ) and its relative trends computed for the 1998 to 2010 period (in parenthesis, in %  $yr^{-1}$ ). Significant trends are in bold text with superscript indicating the level of significance: (a)  $0.05 < p < 0.1$ , (b)  $0.01 < p < 0.05$ , and (c)  $p < 0.01$

Region	May	June	July	August	September
Greenland Sea	3.98 (0.79)	4.41 (−0.32)	2.63 (−0.25)	1.97 (0.05)	1.82 (−0.30)
Norwegian Sea	3.61 (1.69)	3.64 (0.78)	2.84 (0.49)	2.67 (0.40)	2.76 (0.03)
Barents Sea	7.97 (0.51)	3.19 (−0.36)	2.21 ( <b>1.00</b> ) <sup>b</sup>	2.09 ( <b>1.09</b> ) <sup>a</sup>	2.41 (0.25)
Kara Sea	3.58 ( <b>0.19</b> ) <sup>a</sup>	6.11 (−0.25)	6.15 (−0.20)	6.85 (−1.33)	8.95 (−0.01)
Laptev Sea	6.32 (−0.18)	5.57 (0.22)	9.63 (0.27)	9.54 (0.59)	16.06 (−0.01)
East Siberian Sea	3.76 (0.04)	5.54 (0.15)	7.33 (−0.01)	5.65 (0.35)	5.13 (0.14)
Chukchi Sea	6.13 (0.07)	4.58 (1.68)	2.61 (−0.56)	2.53 (0.84)	2.96 ( <b>0.47</b> ) <sup>a</sup>
Beaufort Sea	3.40 (−0.01)	3.32 (−0.35)	3.79 (− <b>0.95</b> ) <sup>b</sup>	3.11 (−1.75)	3.21 (0.11)
Arctic Ocean	5.04 (0.07)	3.66 (0.09)	2.20 (0.02)	1.87 (−0.09)	1.47 (0.20)
Northwestern Passages	2.94 (−0.05)	2.53 (−0.09)	2.33 (− <b>0.53</b> ) <sup>a</sup>	1.94 (− <b>1.02</b> ) <sup>b</sup>	1.78 (−0.13)
Baffin Bay	4.72 (0.29)	2.95 (− <b>1.60</b> ) <sup>a</sup>	2.10 (−0.78)	1.71 (0.08)	1.50 (0.29)
Hudson Bay	4.10 ( <b>0.49</b> ) <sup>c</sup>	3.22 ( <b>1.00</b> ) <sup>b</sup>	2.73 ( <b>1.70</b> ) <sup>b</sup>	2.62 ( <b>1.61</b> ) <sup>b</sup>	2.77 ( <b>0.93</b> ) <sup>b</sup>
Hudson Strait	2.58 (0.43)	3.56 ( <b>0.41</b> ) <sup>b</sup>	3.05 (−0.77)	2.43 (−0.76)	2.33 (0.55)
Davis Strait	5.04 (0.55)	2.47 (0.79)	2.43 (0.57)	2.00 (−0.54)	2.03 (0.20)
Labrador Sea	3.56 (2.04)	3.81 (0.12)	2.85 (0.72)	2.12 (−0.37)	2.11 ( <b>2.21</b> ) <sup>b</sup>
Sea of Okhotsk	6.22 ( <b>1.60</b> ) <sup>b</sup>	5.79 (0.62)	3.26 (1.06)	2.77 ( <b>2.04</b> ) <sup>a</sup>	2.78 ( <b>2.24</b> ) <sup>c</sup>
Bering Sea	5.39 ( <b>1.13</b> ) <sup>b</sup>	4.62 ( <b>4.27</b> ) <sup>b</sup>	3.12 (−0.85)	3.23 (1.15)	3.38 ( <b>1.84</b> ) <sup>c</sup>
Gulf of Alaska	5.41 (1.52)	4.20 (−0.34)	3.31 (0.88)	3.41 ( <b>2.64</b> ) <sup>b</sup>	3.63 (0.80)
<b>Arctic + sub-Arctic Seas</b>	5.13 ( <b>0.99</b> ) <sup>c</sup>	4.15 ( <b>1.18</b> ) <sup>a</sup>	3.34 (0.14)	3.07 ( <b>0.51</b> ) <sup>b</sup>	3.10 ( <b>0.70</b> ) <sup>c</sup>
<b>Circum Arctic</b>	5.17 (0.75)	3.93 (0.16)	3.54 (−0.02)	3.20 (0.09)	3.22 (0.05)

Fig. 5 shows that this observation can only be explained by a change in ocean optical properties, here expressed as the ratio of chlorophyll *a* concentration to the diffuse attenuation coefficient of photo-synthetically usable radiation (CHL/ $K_{PUR}$ ) (Fig. 5; Eq. 5).

In general, low CHL/ $K_{PUR}$  values occurred in stratified, nutrients-depleted surface waters, while high values were found in productive waters sustained by nutrients inputs from rivers or the deep ocean (Fig. 5a–d). In the Canada Basin and Hudson Bay, for example, the haline stratification limits nutrient supply, explaining the low surface CHL (Ferland et al., 2011; Ardyna et al., 2011). In these waters, however, the diffuse attenuation remained relatively important due to the high background in colored detrital materials (CDM) (Granskog et al., 2007; Antoine et al., 2013). In sectors where river inputs are dominant (Kara and Laptev Seas) (Fichot et al., 2013), however, very high values of CHL/ $K_{PUR}$  may be severely overestimated due to the difficulty in distinguishing CHL from other optically active constituents. Improvements of ocean color algorithms for both CHL and  $K_d$  remains a major issue for PP estimation in the coastal arctic (Ben Mustapha et al., 2012).

CHL/ $K_{PUR}$  remained relatively constant within Arctic interior shelves, possibly because sea ice and clouds limit the number of good quality data in these environments. The general rise in CHL/ $K_{PUR}$  observed in permanently open waters during May (Table 4) could be related to increasingly early stabilization of the water column in spring, resulting in ear-

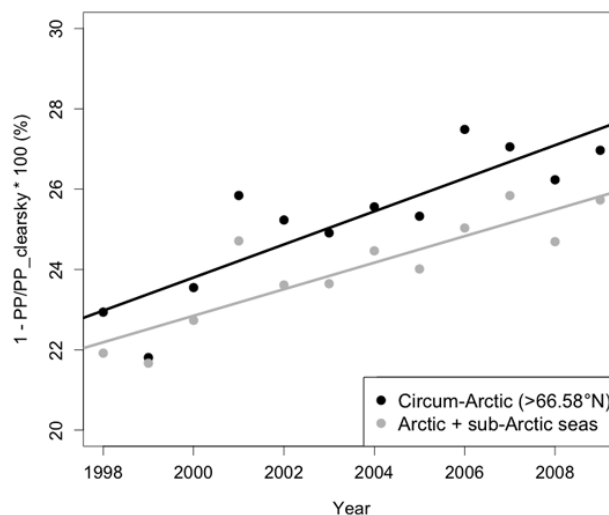


**Fig. 6.** Trends in the potential reduction of total annual PP due to cloudiness (in %) as estimated using  $100 \cdot (1 - PP/PP^{clear\ sky})$  integrated over the circum-Arctic (lat. above  $66.58^\circ N$ ) and over all arctic and subarctic seas.  $PP^{clear\ sky}$  is the total annual PP calculated assuming clear sky conditions. Linear trends statistics are presented in Table 5.

lier phytoplankton blooms (Kahru et al., 2011). The positive PP trends in the Labrador Sea (Fig. 3), for example, are due to increasing values in CHL/ $K_{PUR}$  from south to north in early summer (Fig. 5i, j). Similarly, high PP in the Barents Sea

**Table 5.** Potential reduction of PP due to cloudiness (in %) as estimated using  $100 \cdot (1 - \text{PP}/\text{PP}^{\text{clear sky}})$ , where  $\text{PP}^{\text{clear sky}}$  is the total annual PP calculated assuming clear sky conditions (in parenthesis, in  $\% \text{ yr}^{-1}$ ). Significant trends are in bold text with superscript indicating the level of significance: (a)  $0.05 < p < 0.1$ , (b)  $0.01 < p < 0.05$ , and (c)  $p < 0.01$

Region	Mean 1998–2009 (trends, $\% \text{ yr}^{-1}$ )
Greenland Sea	22.9 ( <b>0.42</b> ) <sup>c</sup>
Norwegian Sea	21.1 ( <b>0.32</b> ) <sup>c</sup>
Barents Sea	26.1 ( <b>0.53</b> ) <sup>c</sup>
Kara Sea	31.7 ( <b>0.36</b> ) <sup>c</sup>
Laptev Sea	32.2 ( <b>0.41</b> ) <sup>c</sup>
East Siberian Sea	26.3 ( <b>0.32</b> ) <sup>c</sup>
Chukchi Sea	19.2 ( <b>0.19</b> ) <sup>a</sup>
Beaufort Sea	21.3 (−0.02)
Arctic Ocean	20.4 (0.22)
Northwestern Passages	16.9 (0.10)
Baffin Bay	19.6 (−0.29)
Hudson Bay	22.5 ( <b>0.19</b> ) <sup>a</sup>
Hudson Strait	18.3 (0.11)
Davis Strait	20.5 (0.17)
Labrador Sea	20.6 (0.01)
Sea of Okhotsk	22.6 (0.09)
Bering Sea	24.8 ( <b>0.35</b> ) <sup>c</sup>
Gulf of Alaska	21.4 (0.27)
<b>Arctic + sub-Arctic Seas</b>	24.0 ( <b>0.33</b> ) <sup>c</sup>
<b>Circum Arctic</b>	25.2 ( <b>0.36</b> ) <sup>b</sup>

(Table 3) is mostly driven by positive trends in  $\text{CHL}/\text{K}_{\text{PUR}}$  in May ( $15 \text{ mg C m}^{-2} \text{ d}^{-1}$ )  $\text{yr}^{-1}$ ) (Fig. 5j, k; Table 4).

Despite a general positive trend in PP over much of the Arctic, we found strong indications that total annual PP is declining in regions of prime ecological importance. Negative PP trends were mostly explained by a reduction of PAR due to increasing cloudiness (Fig. 1) in the northern Bering Sea (Fig. 3) and by higher SIC and lower penetration of sun light in the water column (Fig. 2) near the location of the northeast water (NEW) polynya. The latter result may be due to an increase in sea-ice export through Fram Strait since 2003 as reported recently by Kwok et al. (2009). The North Water (NOW) polynya, located in the northern Baffin Bay, experienced one of the most severe drop in PP ( $5 \text{ gC m}^{-2} \text{ yr}^{-1}$ ; Fig. 4b). With an area of  $80\,000 \text{ km}^2$ , the NOW has been considered to be the most productive recurrent polynya north of  $77^\circ \text{ N}$  due to a long and intense diatom bloom that starts in May and fuels a rich marine ecosystem supporting polar cods, large aggregations of marine mammals, sea birds and polar bears (Tremblay et al., 2006). Our results indicate that the timing of the phytoplankton bloom have changed over time. Indeed, an increase in  $\text{CHL}/\text{K}_{\text{PUR}}$  in May was followed by a sustained decrease in June and July (Fig. 5), which was primarily responsible for the decline in the annual productivity of the NOW. Recent evidence from Arctic bivalves liv-

ing at depth  $\sim 600 \text{ m}$  suggested that a dramatic increase in the export of freshly produced organic matter in the euphotic zone to the deep ocean has occurred during the last decade (Gaillard et al., 2013). The authors suggested that this major ecosystem shift is primarily caused by changing local sea ice dynamics and/or match-mismatch between phytoplankton bloom and zooplankton grazing. The earlier timing of the phytoplankton bloom, which may escape zooplankton grazing, raise questions about the ultimate drivers of changes in the NOW. They could be due to changes in the quantity or properties (e.g. salinity, nutrients) of the in-flow of cold, nutrient-depleted waters coming from the Arctic Ocean (Kwok et al., 2010; Münchow et al., 2011), or in altered forcings from the atmosphere or the ocean.

Important limitations of our satellite-based PP trends assessment must be mentioned. Firstly, our method cannot detect if changes occurred in the subsurface chlorophyll *a* maximum (SCM), which can be important in the Arctic waters during the summer period (Martin et al., 2012). Recent studies, however, suggested that the error in the annual PP assessment resulting from the omission of the SCM is small, but more important during the post-bloom period in late summer in stratified seas (Ardyna et al., 2013; Arrigo et al., 2011). Secondly, under-ice phytoplankton blooms, which are undetectable from space, may be more important than previously thought. These blooms have been observed in different Arctic sectors and can locally represent most of the annual PP (Arrigo et al., 2012; Mundy et al., 2009). With the reduction of the sea ice thickness under warming climate conditions (Kwok et al., 2009), under-ice phytoplankton blooms may be expanding but not yet quantified. Thirdly, the ocean color time series remains relatively short (i.e. 13 yr) for the assessment of long-term trends in the ocean productivity. But the pace at which changes are occurring in the Arctic may hide the natural variability due to decadal oscillations.

High spatial resolution maps of PP trends, together with those in  $\text{PAR}(0+)$ ,  $\text{PAR}(0-)$  and  $\text{CHL}/\text{K}_{\text{PUR}}$ , provide new insights into the main drivers of changes in primary productivity across the Arctic and sub-Arctic marine ecosystems. Future developments of long-term monitoring capabilities of marine arctic ecosystems should, among other, (1) include improvements in the ocean color algorithms to reduce the uncertainty on the satellite-based PP estimations in optically complex waters, in particular, in the river-influenced ocean margins, (2) address the problem of data continuity to produce consistent time series of ocean color and other sensors, (3) evaluate and compare methods used to estimate PAR reaching the sea surface under cloud and ice conditions and (4) examine in more details the environmental variability to better understand the most important drivers of changes in the ocean optical properties and PP. Among those, changes in mixed layer depth, which is crucial for the supply of nutrients in the euphotic zone must be monitored with respect to the potential impact of sea surface warming and/or increased freshwater input resulting from ice loss,

precipitation, or river discharge. On the other hand, increases in the frequency of cyclones in late summer could enhanced regional upwelling and PP. Finally, the linkage of the PP to large scale atmospheric oscillations such as North Atlantic Oscillation, Arctic Oscillation, Pacific decadal Oscillation, to name but a few, should be examined more deeply.

**Supplementary material related to this article is available online at:** <http://www.biogeosciences.net/10/4087/2013/bg-10-4087-2013-supplement.pdf>.

*Acknowledgements.* This work was supported by a NSERC discovery grant to S. Bélanger and a WWF-Canada contract to Arctus inc. The authors are grateful to James Snider and Peter Ewins from WWF-Canada and Servet Cizmeli and Laurens Put from Arctus inc. for their contributions to the study at its early stage. They also acknowledge the NASA Ocean Color team for providing SeaWiFS data and S. Maritorena for access to GSM data, as well as X. Zhang from the ISCCP project for provision of the surface fluxes data products. This is a contribution to the ArcticNet and Malina programs.

Edited by: E. Boss

## References

- Antoine, D., Hooker, S. B., Bélanger, S., Matsuoka, A., and Babin, M.: Apparent optical properties of the Canadian Beaufort Sea – Part 1, *Biogeoscience Discuss.*, 10, 4025–4065, doi:10.5194/bgd-10-4025-2013, 2013.
- Ardyna, M., Gosselin, M., Michel, C., Poulin, M., and Tremblay, J.-E.: Environmental forcing of phytoplankton community structure and function in the Canadian High Arctic: contrasting oligotrophic and eutrophic regions, *Mar. Ecol. Progr. Series*, 442, 37–57, doi:10.3354/meps09378, 2011.
- Ardyna, M., Babin, M., Gosselin, M., Devred, E., Bélanger, S., Matsuoka, A., and Tremblay, J.-É.: Parameterization of vertical chlorophyll a in the Arctic Ocean: impact of the subsurface chlorophyll maximum on regional, seasonal and annual primary production estimates, *Biogeosciences Discuss.*, 10, 1345–1399, doi:10.5194/bgd-10-1345-2013, 2013.
- Arrigo, K. R. and van Dijken, G. L.: Secular trends in Arctic Ocean net primary production, *J. Geophys. Res.*, 116, C09011, doi:10.1029/2011JC007151, 2011.
- Arrigo, K. R., Worthen, D., Schnell, A., and Lizotte, M. P.: Primary production in Southern Ocean waters, *J. Geophys. Res.*, 103, 15587–15600, 1998.
- Arrigo, K. R., van Dijken, G., and Pabi, S.: Impact of a shrinking Arctic ice cover on marine primary production, *Geophys. Res. Lett.*, 35, L19603, doi:10.1029/2008GL035028, 2008.
- Arrigo, K. R., Matrai, P. A., and van Dijken, G. L.: Primary productivity in the Arctic Ocean: impacts of complex optical properties and subsurface chlorophyll maxima on large-scale estimates, *J. Geophys. Res.*, 116, C110022, doi:10.1029/2011JC007273, 2011.
- Arrigo, K. R., Perovich, D. K., Pickart, R. S., Brown, Z. W., van Dijken, G. L., Lowry, K. E., Mills, M. M., Palmer, M. A., Balch, W. M., Bahr, F., Bates, N. R., Benitez-Nelson, C., Bowler, B., Brownlee, E., Ehn, J. K., Frey, K. E., Garley, R., Laney, S. R., Lubelczyk, L., Mathis, J., Matsuoka, A., Mitchell, B. G., Moore, G. W. K., Ortega-Retuerta, E., Pal, S., Polashenski, C. M., Reynolds, R. A., Schieber, B., Sosik, H. M., Stephens, M., and Swift, J. H.: Massive Phytoplankton Blooms Under Arctic Sea Ice, *Science*, 336, 1408, doi:10.1126/science.1215065, 2012.
- Behrenfeld, M. J., Malley, R. T. O., Siegel, D. A., McClain, C. R., Sarmiento, J. L., Feldman, G. C., Milligan, A. J., Falkowski, P. G., Letelier, R. M., and Boss, E. S.: Climate-driven trends in contemporary ocean productivity, *Nature*, 444, 752–755, doi:10.1038/nature05317, 2006.
- Ben Mustapha, S., Larouche, P., and Bélanger, S.: Evaluation of ocean color algorithms in the Southeastern Beaufort Sea: new parameterization using SeaWiFS, MODIS and MERIS spectral bands, *Can. J. Remote Sens.*, 54, 535–556, 2012.
- Bélanger, S.: Response of light-related carbon fluxes in the Arctic Ocean to climate change: quantification and monitoring of dissolved organic matter photo-oxidation in the Beaufort Sea using satellite remote sensing, PhD thesis, Université Pierre et Marie Curie, Paris, France, 243 pp., 2006.
- Bélanger, S., Babin, M., and Larouche, P.: An empirical ocean color algorithm for estimating the contribution of chromophoric dissolved organic matter to total light absorption in optically complex waters, *J. Geophys. Res.*, 113, C04027, doi:10.1029/2007JC004436, 2008.
- Bricaud, A., Morel, A., Babin, M., Allali, K., and Claustre, H.: Variations of Light Absorption by Suspended Particles with Chlorophyll a Concentration in Oceanic (case 1) Waters: Analysis and Implications for Bio-optical Models., *J. Geophys. Res.*, 103, C13, 31033–31044, 1998.
- Carmack, E. C. and Chapman, D. C.: Wind-driven shelf/basin exchange on an Arctic shelf: the joint roles of ice cover extent and shelf-break bathymetry, *Geophys. Res. Lett.*, 30, 1778, doi:10.1029/2003GL017526, 2003.
- Cavalieri, D. J., Parkinson, C., Gloersen, P., and Zwally, H. J.: Sea Ice Concentrations from Nimbus-7 SMMR and DMSP SSM/I Passive Microwave Data, (1998–2007), 1996.
- Chernokulsky, A. and Mokhov, I. I.: Climatology of total cloudiness in the Arctic: an intercomparison of observations and reanalyses, *Adv. Meteorol.*, 2012, 1–15, doi:10.1155/2012/542093, 2012.
- Comiso, J. C., Parkinson, C. L., Gersten, R., and Stock, L.: Accelerated decline in the Arctic sea ice cover, *Geophys. Res. Lett.*, 35, 1–6, doi:10.1029/2007GL031972, 2008.
- Eastman, R. and Warren, S. G.: Interannual variations of Arctic cloud types in relation to sea ice, *J. Climate*, 23, 4216–4232, doi:10.1175/2010JCLI3492.1, 2010.
- Ferland, J., Gosselin, M., and Starr, M.: Environmental control of summer primary production in the Hudson Bay system: The role of stratification, *Journal of Marine Systems*, 88, 385–400, doi:10.1016/j.jmarsys.2011.03.015, 2011.
- Fichot, C. G., Kaiser, K., Hooker, S. B., Amon, R. M. W., Babin, M., Bélanger, S., Walker, S. A., and Benner, R.: Pan-Arctic Distributions of Continental Runoff in the Arctic Ocean. *Sci. Rep.* 3, 1053, doi:10.1038/srep01053, 2013.
- Frey, K. E. and Smith, L. C.: Amplified carbon release from vast West Siberian peatlands by 2100, *Geophys. Res. Lett.*, 32,

- L09401, doi:10.1029/2004GL022025, 2005.
- Gaillard, B., Olivier, F., Thébault, J., Meziane, T., Tremblay, R., Dumont, D., Bélanger, S., Gosselin, M., Chauvaud, L., Martel, A. L., and Archambault, P.: Bathyal Arctic bivalves benefit from climate changes, submitted, 2013.
- Granskog, M. A., Macdonald, R. W., Mundy, C.-J., and Barber, D. G.: Distribution, characteristics and potential impacts of chromophoric dissolved organic matter (CDOM) in Hudson Strait and Hudson Bay, Canada, *Cont. Shelf Res.*, 27, 2032–2050, doi:10.1016/j.csr.2007.05.001, 2007.
- Grebmeier, J. M., Overland, J. E., Moore, S. E., Farley, E. V., Carmack, E. C., Cooper, L. W., Frey, K. E., Helle, J. H., McLaughlin, F. A., and McNutt, S. L.: A major ecosystem shift in the Northern Bering Sea, *Science*, 311, 1461–1464, 2006.
- Harrison, W. G. and Platt, T.: Photosynthesis-irradiance relationships in polar and temperate phytoplankton populations, *Polar Biol.*, 5, 153–164, 1986.
- Huot, Y., Babin, M., and Bruyant, F.: Photosynthetic parameters in the Beaufort Sea in relation to the phytoplankton community structure, *Biogeosciences*, 10, 3445–3454, doi:10.5194/bg-10-3445-2013, 2013.
- Kahru, M., Brotas, V., Manzano-Sarabia, M., and Mitchell, B. G.: Are phytoplankton blooms occurring earlier in the Arctic?, *Glob. Change Biol.*, 17, 1733–1739, doi:10.1111/j.1365-2486.2010.02312.x, 2011.
- Kwok, R., Cunningham, G. F., Wensnahan, M., Rigor, I., Zwally, H. J., and Yi, D.: Thinning and volume loss of the Arctic Ocean sea ice cover: 2003–2008, *J. Geophys. Res.*, 114, C07005, doi:10.1029/2009JC005312, 2009.
- Kwok, R., Toudal Pedersen, L., Gudmandsen, P., and Pang, S. S.: Large sea ice outflow into the Nares Strait in 2007, *Geophys. Res. Lett.*, 37, L03502, doi:10.1029/2009GL041872, 2010.
- Lee, Z.-P., Carder, K. L., and Arnone, R. A.: Deriving inherent optical properties from water color: a multiband quasi-analytical algorithm for optically deep waters, *App. Opt.*, 41, 5755–5772, 2002.
- Lee, Z. P., Du, K. P., and Arnone, R.: A model for the diffuse attenuation coefficient of downwelling irradiance, *J. Geophys. Res.*, 110, C02016, doi:10.1029/2004JC002275, 2005.
- Li, W. K. W., McLaughlin, F. A., Lovejoy, C., and Carmack, E. C.: Smallest algae thrive as the Arctic Ocean freshens, *Science*, 326, 539, doi:10.1126/science.1179798, 2009.
- Maritorena, S., Siegel, D. A., and Peterson, A. R.: Optimization of a semi-analytical ocean color model for global-scale applications, *App. Opt.*, 41, 2705–2714, 2002.
- Martin, J., Tremblay, J.-E., Gagnon, J., Tremblay, G., Lapoussiere, A., Jose, C., Poulin, M., Gosselin, M., Gratton, Y., and Michel, C.: Prevalence, structure and properties of subsurface chlorophyll maxima in Canadian Arctic waters, *Mar. Ecol. Progr. Ser.*, 412, 69–84, doi:10.3354/meps08666, 2010.
- Maslanik, J. A. and Stroeve, J. C.: Near-Real-Time DMSP SSM/I-SSMIS Daily Polar Gridded Sea Ice Concentrations, (2008–2010), Boulder, Colorado USA: National Snow and Ice Data Center, Digital media, 1999.
- Matsuoka, A., Huot, Y., Shimada, K., Saitoh, S.-I., and Babin, M.: Bio-optical characteristics of the Western Arctic Ocean: implications for ocean color algorithms, *Can. J. Remote Sens.*, 33, 503–518, 2007.
- Matsuoka, A., Hill, V., Huot, Y., Babin, M., and Bricaud, A.: Seasonal variability in the light absorption properties of Western Arctic waters: parameterization of the individual components of absorption for ocean color applications, *J. Geophys. Res.*, 116, 1–15, doi:10.1029/2009JC005594, 2011.
- Morel, A. and Maritorena, S.: Bio-optical Properties of Oceanic Waters: A Reappraisal, *J. Geophys. Res.*, 106, 7163–7180, 2001.
- Morel, A.: Available, Usable, and Stored Radiant Energy in Relation to Marine Photosynthesis, *Deep-Sea Res.*, 25, 673–688, 1978.
- Morel, A.: Light and marine photosynthesis: a spectral model with geochemical and climatological implications, *Prog. Oceanogr.*, 26, 263–306, 1991.
- Münchow, A., Falkner, K. K., Melling, H., Rabe, B., and Johnson, H. L.: Ocean warming and freshening of Nares Strait bottom waters off NW Greenland 2003–09, *Oceanography*, 24, 114–123, doi:10.5670/oceanog.2011.62, 2011.
- Mundy, C. J., Gosselin, M., Ehn, J., Gratton, Y., Rossnagel, A., Barber, D. G., Martin, J., Tremblay, J.-É., Palmer, M., Arrigo, K. R., Darnis, G., Fortier, L., Else, B., and Papakyriakou, T.: Contribution of under-ice primary production to an ice-edge upwelling phytoplankton bloom in the Canadian Beaufort Sea, *Geophys. Res. Lett.*, 36, L17601, doi:10.1029/2009GL038837, 2009.
- Palm, S. P., Strey, S. T., Spinhirne, J., and Markus, T.: Influence of Arctic sea ice extent on polar cloud fraction and vertical structure and implications for regional climate, *J. Geophys. Res.*, 115, 1–9, doi:10.1029/2010JD013900, 2010.
- Perovich, D. K., Light, B., Eicken, H., Jones, K. F., Runciman, K., and Nghiem, S. V.: Increasing solar heating of the Arctic Ocean and adjacent seas, 1979–2005: attribution and role in the ice-albedo feedback, *Geophys. Res. Lett.*, 34, L19505, doi:10.1029/2007GL031480, 2007.
- Perrette, M., Yool, A., Quartly, G. D., and Popova, E. E.: Near-ubiquity of ice-edge blooms in the Arctic, *Biogeosciences*, 8, 515–524, doi:10.5194/bg-8-515-2011, 2011.
- Peterson, B. J., McClelland, J. W., Curry, R., Holmes, R. M., Walsh, J. E., and Aagaard, K.: Trajectory shifts in the Arctic and Subarctic freshwater cycle, *Science*, 313, 1061–1066, 2006.
- Platt, T. and Sathyendranath, S.: Estimators of Primary Production for Interpretation of Remotely Sensed Data on Ocean Color, *J. Geophys. Res.*, 98, 14561–14576, 1993.
- Platt, T., Gallegos, C. L., and Harrison, W. G.: Photoinhibition of photosynthesis in natural assemblages of marine phytoplankton, *J. Mar. Res.*, 38, 687–701, 1980.
- Rachold, V., Grigoriev, M. N., Are, F. E., Solomon, S., Reimnitz, E., Kassens, H., and Antonow, M.: Coastal erosion vs riverine sediment discharge in the Arctic Shelf Seas, *Int. J. Earth Sci.*, 89, 450–460, doi:10.1007/s005310000113, 2000.
- Ricchiazzi, P., Yang, S. R., Gautier, C., and Sowle, D.: SBDART: a research and teaching software tool for plane-parallel radiative transfer in the Earth atmosphere, *B. Am. Meteorol. Soc.*, 79, 2101–2114, 1998.
- Sathyendranath, S., Platt, T., Caverhill, C. M., Warnock, R. E., and Lewis, M. R.: Remote sensing of oceanic primary production: computations using a spectral model, *Deep-Sea Res.*, 36, 431–453, 1989.
- Schweiger, A. J., Lindsay, R. W., Key, J. R., and Francis, J. A.: Arctic clouds in multiyear satellite data sets, *Geophys. Res. Lett.*, 26, 1845, doi:10.1029/1999GL900479, 1999.

- Siegel, D., Maritorena, S., Nelson, N. B., Behrenfeld, M. J., and McClain, C. R.: Colored dissolved organic matter and its influence on the satellite-based characterization of the ocean biosphere, *Geophys. Res. Lett.*, 32, L20605, doi:10.1029/2005GL024310, 2005.
- Smyth, T. J., Tilstone, G. H., and Groom, S. B.: Integration of radiative transfer into satellite models of ocean primary production, *J. Geophys. Res.*, 110, C10014, doi:10.1029/2004JC002784, 2005.
- Tremblay, J.-É. and Gagnon, J.: The effects of irradiance and nutrient supply on the productivity of Arctic waters: a perspective on climate change, in: Influence of climate change on changing Arctic and sub-arctic conditions, edited by: Nihoul, J. C. J. and Kostianoy, A. G., 73–89, Springer, 2009.
- Tremblay, J. E., Hattori, H., Michel, C., Ringuette, M., Mei, Z.-P., Lovejoy, C., Fortier, L., Hobson, K. A., Amiel, D., and Cochran, J. K.: Trophic structure and pathways of biogenic carbon flow in the Eastern North Water Polynya, *Prog. Oceanogr.*, 71, 402–425, 2006.
- Tremblay, J.-É., Bélanger, S., Barber, D. G., Asplin, M., Martin, J., Darnis, G., Fortier, L., Gratton, Y., Link, H., Archambault, P., Sallon, A., Michel, C., Williams, W. G., Philippe, B., and Goselin, M.: Climate forcing multiplies biological productivity in the coastal Arctic Ocean, *Geophys. Res. Lett.*, 38, L18604, doi:10.1029/2011GL048825, 2011.
- Vavrus, S., Holland, M. M., and Bailey, D. A.: Changes in Arctic clouds during intervals of rapid sea ice loss, *Clim. Dynam.*, 36, 1475–1489, doi:10.1007/s00382-010-0816-0, 2010.
- Wang, X. and Key, J. R.: Arctic surface, cloud, and radiation properties based on the AVHRR Polar Pathfinder dataset, Part II: recent trends, *J. Climate*, 18, 2575–2593, 2005.
- Wang, J., Cota, G., and Ruble, D. A.: Absorption and backscattering in the Beaufort and Chukchi Seas, *J. Geophys. Res.*, 110, C04014, doi:10.1029/2002JC001653, 2005.
- Zhang, X., Vincent, L. A., Hogg, W. D., and Niitsoo, A.: Temperature and precipitation trends in Canada during the 20th Century, *Atmos. Ocean*, 38, 395–429, 2000.
- Zhang, Y. C., Rossow, W. B., Lacis, A. A., Oinas, V., and Mishchenko, M. I.: Calculation of radiative fluxes from the surface to top of atmosphere based on ISCCP and other global data sets: refinements of the radiative transfer model and the input data, *J. Geophys. Res.*, 109, D19105, doi:10.1029/2003JD004457, 2004.